

Article

Properties and Microstructure of a Cement-Based Capillary Crystalline Waterproofing Grouting Material

Mengjie Wang ¹, Xiaohua Yang ^{1,*} , Kunlong Zheng ² and Rui Chen ¹

¹ School of Highway, Chang'an University, Xi'an 710064, China; 2021021004@chd.edu.cn (M.W.); rchenhua@chd.edu.cn (R.C.)

² China State Construction Silk Road Investment Group Co., Ltd., Xi'an 710075, China; kunlongzheng@163.com

* Correspondence: xiaohuay@126.com; Tel.: +86-029-82334453

Abstract: Cement grout is traditionally used for treating water leakage distress in tunnels. However, traditional cement grout has the disadvantages of a poor anti-seepage performance, long setting time, and slow strength gain. To this end, a high-performance cement-based capillary crystalline waterproofing (CCCW) grouting material was synthesized using cement, capillary crystalline material, and several admixtures. The influences of the material proportions on the viscosity, bleeding rate, and setting time of the fresh grout, as well as the permeability coefficient of the grouted aggregate and the unconfined compression strength of the hardened grout material, were systematically studied. The mineralogy and microstructure of the CCCW grouting material were examined using X-ray diffraction, industrial computed tomography, and scanning electron microscopy. The results indicated that the capillary crystalline material PNC803 was not suitable for mixing with bentonite, sodium chloride, and triethanolamine in cementitious slurries, but it can produce excellent synergistic effects with sulfate, calcium chloride, and triisopropanolamine. An analysis of the microstructure of the CCCW grouting material showed that the PNC803 and additives can promote the hydration of cement, which yields more hydration products, sealing water passage and filling micro voids and therefore leading to enhanced waterproofing and strengthening effects. These research results could improve the applicability of CCCW material in tunnel engineering.



Citation: Wang, M.; Yang, X.; Zheng, K.; Chen, R. Properties and Microstructure of a Cement-Based Capillary Crystalline Waterproofing Grouting Material. *Buildings* **2024**, *14*, 1439. <https://doi.org/10.3390/buildings14051439>

Academic Editors: Haoxin Li and Nicolas Ali Libre

Received: 5 March 2024

Revised: 21 April 2024

Accepted: 15 May 2024

Published: 16 May 2024



Copyright: © 2024 by the authors. Licensee MDPI, Basel, Switzerland. This article is an open access article distributed under the terms and conditions of the Creative Commons Attribution (CC BY) license (<https://creativecommons.org/licenses/by/4.0/>).

1. Introduction

When a tunnel passes through water-bearing stratum, it is extremely susceptible to water-related distresses such as water leakage and water inrush [1,2] if pre-term preventive measures or initial disposal methods were not well implemented. These water-related distresses, which directly affect the regular operation of tunnels, are urgent engineering and technical problems that must be addressed. The grouting method is generally adopted for solving these problems, and the grouting effect largely depends on the selection of grouting materials.

Many researchers have conducted studies on grouting materials. Chakrabarti et al. [3], Nosrati et al. [4], and Zhang et al. [5] improved a clay slurry, resulting in significant changes in the rheological properties and strength compared with traditional clay slurry. Yang et al. [6] and Ye et al. [7] systematically studied grouting parameters such as the proportion, grouting pressure, and slurry diffusion radius of cement–water glass grouting materials and achieved good grouting reinforcement effects in tunnel engineering. To improve the permeability of cement slurry, Li et al. [8], Mozumder et al. [9], Shin et al. [10], and Sha et al. [11] prepared various ultrafine cement-based grouting materials and established a slurry permeability prediction model based on artificial neural networks. Li et al. [12] and Yan et al. [13] analyzed the reaction mechanism of acrylic grouting materials and added

different types of accelerators to prepare various acrylic slurries with a strong stability and impermeability. Wang et al. [14], Wang et al. [15], and Liu et al. [16] investigated the film-forming status of a high-permeability epoxy slurry and its penetration depth into concrete. Nautts [17], Saleh et al. [18], and Hao et al. [19] reported that polyurethane materials have a high degree of curing and strong erosion resistance. Sun et al. [20], Zheng et al. [21], and Li et al. [22] studied the basic properties of a cementitious capillary crystalline waterproofing (CCCW) material and explored its feasibility for treating tunnel leakage diseases. Ebigo et al. [23] and Van Wijngaarden et al. [24] used a microbial-induced calcium carbonate precipitation to solidify sandy soil and combined experimental and numerical simulations to study the bacterial behavior, distribution of calcium carbonate, and changes in permeability. Dong et al. [25] and Zheng et al. [26] developed microcapsule self-healing materials and analyzed their performance characteristics and repair mechanisms.

However, traditional cement-based grouting materials cannot form molecular-level connections with concrete and can only be wrapped in a shell-like manner, which is prone to failure when the water pressure around the concrete lining increases [20]. Polymeric chemical materials have good injectability, but they are highly toxic to humans and the environment. The research and development of microbial and micro-capsule materials are still in their early stages, and their preparation costs are relatively high [1]. Recently, the momentum for CCCW development has rapidly increased. This material performs well in self-healing, cost-effectiveness, and environmental friendliness [27]. CCCW material is a powder-like, rigid, waterproof material made of cement, quartz sand, a variety of active chemicals, and other auxiliary materials [28,29]. Unlike other waterproof materials, this material can not only be used for waterproofing treatment of the positive and negative sides of concrete structures but also be directly added to concrete for use [30]. It is frequently utilized in numerous waterproofing engineering projects, including sewage treatment plants and reservoirs, and it has produced positive results because of its unique waterproof capabilities [31,32]. However, the material has been rarely used in underground space engineering, such as tunnels, and it is still in the promotion stage. Compared with cement slurries, capillary crystalline slurries significantly improve the concretion rate. However, no significant change occurs in performance aspects such as viscosity, setting time, and early compression strength [21]. As a tunnel anti-seepage grouting material, it not only must be impermeable to prevent leakage, but it must also have good fluidity to diffuse to a certain depth into microcracks. Additionally, problems such as poor water-blocking effects caused by long setting times and slow strength gain must be avoided. Therefore, this study aims to introduce CCCW material into underground space engineering and obtain a green grouting material with a stable performance and good durability to solve tunnel water leakage problems. In this article, cement, CCCW material, and several admixtures were used as raw materials to prepare a high-performance cement-based capillary crystalline grouting material with an outstanding anti-seepage ability and comprehensive performance. The action mechanism of this material was explored from the perspective of the hydration products and microstructure.

2. Materials and Methods

2.1. Materials

The cement used in this experiment was PO 42.5 ordinary Portland cement (OPC), provided by Fenyi Conch Cement Co., Ltd., Xinyu, China. The CCCW material used was Penetron Admix (PNC803) provided by Beijing Penetron International Building Materials Co., Ltd., Beijing, China. In addition, to obtain a slurry with a better comprehensive performance, multiple commonly used cement admixtures were chosen for comparison purposes. Bentonite was used to improve the stability and reduce the bleeding rate of the slurry, and sodium sulfate was used to reduce the viscosity and improve the fluidity. Sodium chloride combined with triethanolamine (TEA) or calcium chloride and triisopropanolamine (TIPA) was used to control the setting time and improve the early strength of the grouted material.

The cement admixtures were provided by Wuxi Yatai United Chemical Co., Ltd., Wuxi, China. Laboratory tap water was used as the mixing water.

2.2. Experimental Design

In tunnel grouting engineering, the water–cement ratio is often relatively high to ensure the groutability of the slurry. The water–cement ratio in the experiment was fixed at 1:1 to match the actual engineering conditions. At present, as the active chemical composition of PNC803 is unknown, it is unclear whether it can synergize with various cement admixtures. Therefore, preliminary experiments were conducted. PNC803 was separately mixed with different cement admixtures, and the effects of each combination were assessed in a targeted manner. The specific experimental contents are listed in Table 1.

Table 1. Pre-experimental design.

No.	PNC803 (%)	Bentonite (%)	Na ₂ SO ₄ (%)	NaCl (%)	TEA (%)	CaCl ₂ (%)	TIPA (%)	Response
OPC P	— 4	—	—	—	—	—	—	Viscosity, bleeding rate, setting time, unconfined compression strength
X XP	4	10 10						Bleeding rate
S SP	4		0.8 0.8					Viscosity, bleeding rate
N NP C CP	4			1.0 1.0	0.05 0.05	2.0 2.0	0.05 0.05	Bleeding rate, setting time, unconfined compression strength

Note: The dosage of each additive in the table is the percentage of the additive mass relative to the cement mass.

Through the pre-experimental determination of a suitable additive type, the mix proportion of the high-performance capillary crystalline anti-seepage grouting material was designed using orthogonal experiments. Using the viscosity, bleeding rate, setting time, permeability coefficient, and unconfined compression strength as parameter indicators, this paper determined the primary and secondary impact relationships of PNC803 and cement admixtures on the basic properties of the cement slurry, permeability of the grouted aggregate, and physical properties of the hardened grouting material, and it also analyzed the main influencing factors. The phase composition, pore structure, and micromorphology of the samples were analyzed using X-ray diffraction (XRD), industrial computed tomography (CT), and scanning electron microscopy (SEM).

2.3. Test Methods

2.3.1. Viscosity Test

The viscosity affects the fluidity, diffusion range, and degree of penetration of the slurry. Referring to standard JJJ 1002-2005 [33], the viscosity of each group of slurries was measured using an NDJ-1 rotary viscometer. Rotor No. 1 was selected, and the rotation speed was 6 r/min.

2.3.2. Bleeding Rate Test

The bleeding rate of the grouting slurry refers to the percentage of water separated from the slurry to the total volume of the original slurry within a certain time period and under certain conditions. The higher the percentage, the poorer the stability of the slurry. The bleeding rate directly affects the uniformity of the slurry and its mechanical properties after hardening. Referring to standard JTG 3420-2020 [34], each group of evenly mixed fresh slurries, V_0 (mL), was injected into graduated cylinders using a needle tube. The scale between the upper clarified water and the lower precipitated colloid was read every 0.5 h.

After the reading stabilized, the bleeding volume V_1 (mL) of the different slurry groups was recorded, and the bleeding rate, $m = V_1/V_0 \times 100\%$, was calculated.

2.3.3. Setting Time Test

The setting time is related to the diffusion range and the distribution of the slurry in the injected medium. Referring to standard GB/T 1346-2011 [35], the initial and final setting times of each group of slurries were measured using a Vicat apparatus.

2.3.4. Permeability Test

The permeability coefficient directly reflects the grouting body permeability. To simulate the grouting situation in actual engineering, in this experiment, each group of evenly mixed slurries was injected into the aggregate with a particle size of 5–15 mm to create the frustum of a cone-shaped impermeable specimen (with a top diameter of 175 mm, bottom diameter of 185 mm, and height of 150 mm), with every six specimens comprising a group. Referring to standard JTG 3420-2020 [34], the permeability coefficient of each group of grouting bodies cured for 7 and 28 d was measured using an HP-4.0 concrete permeability meter. During the experiment, the water pressure was controlled at 1.2 MPa.

2.3.5. Unconfined Compression Strength Test (UCS)

The unconfined compression strength is an important mechanical property of hardened grouting material. In this experiment, fresh slurry was poured into a 70.7 mm × 70.7 mm × 70.7 mm cubic test mold. Referring to standard GB/T 50081-2019 [36], the unconfined compression strength of each group of slurry stone bodies cured for 3, 7, and 28 d was measured using a universal testing machine loaded at a speed of 0.5 MPa/s.

2.3.6. XRD

To observe the changes in the phase composition of the solidified slurry, XRD was performed on the cement slurry and capillary crystalline slurry solidified samples, respectively. In this experiment, the materials were sampled, ground, sieved, numbered, and then placed in an AXS D8 ADVANCE X-ray diffractometer for phase composition detection using a scanning speed of 5°/min and a scanning range of 5°–80° (2θ).

2.3.7. CT

The pore structure affects the compactness, strength, and durability of the structure. The equipment used was YXLON Y.CT Modular, with a peak power of 320 W, a peak voltage of 225 kV, a peak current of 3.0 mA, and a spatial resolution of 23.0 LP/mm. In this experiment, the slurry was injected into the aggregate with a particle size of 5–15 mm to produce 70.7 mm × 70.7 mm × 70.7 mm cubic grouted stones to observe the pore structure characteristics in the grouted material. After curing for 3, 7, and 28 d, the specimens were dried, and a CT scan was performed to analyze the pore characteristic parameters such as porosity and pore distribution.

2.3.8. SEM

To further understand the microstructure and evaluate the material properties and mechanisms of action, SEM was performed on the samples. In this experiment, the hardened grouting materials after curing for 28 d were crushed, sampled, numbered, dried, sprayed with gold, and vacuum-treated before being placed in a Hitachi S-4800 scanning electron microscope for the analysis and observation of the growth of crystalline substances. The testing equipment and processes are shown in Figure 1.

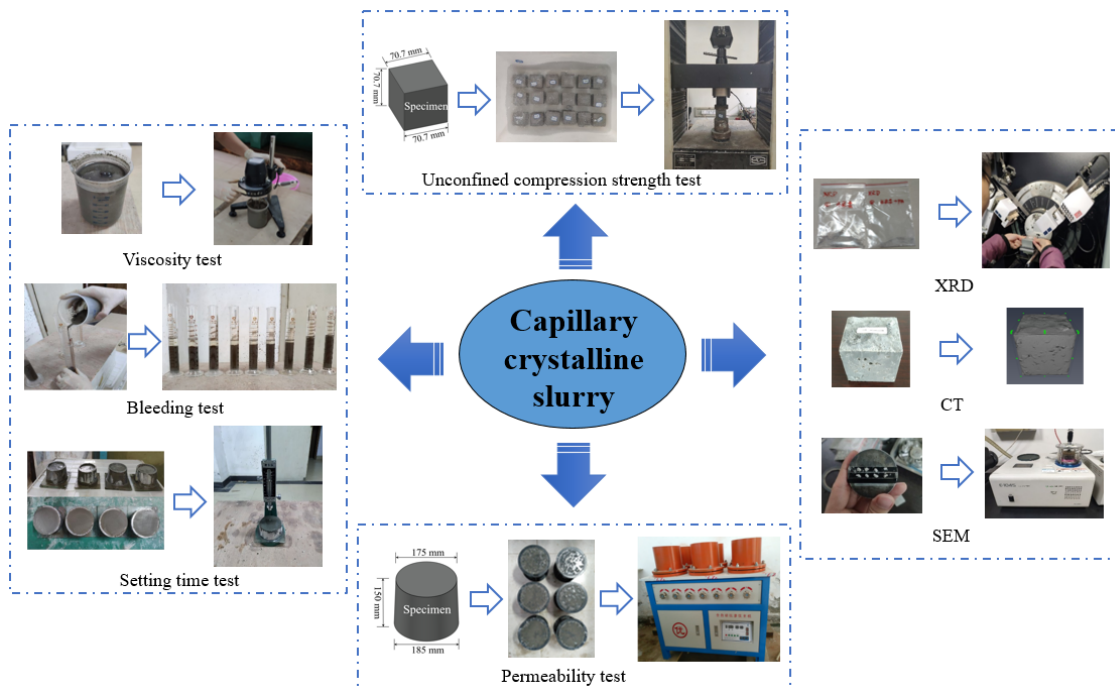


Figure 1. Testing equipment and processes.

3. Results and Discussion

3.1. Pre-Experiment

Figure 2a shows that the bleeding rate of the X group cement slurry with only bentonite was 17.0%, that of the P group cement slurry with only PNC803 was 2.6%, and that of the XP group cement slurry with both PNC803 and bentonite was 15.7%. Thus, in terms of improving the stability of the cement slurry, adding only PNC803 had a better effect than adding only bentonite. More importantly, the addition of bentonite did not reduce the water precipitation rate of the capillary crystalline cement slurry further. This may be because when bentonite and PNC803 act together in the cement slurry, bentonite envelops the active substances in PNC803 because of its water absorption and expansion, thereby affecting the effectiveness of the active substances. In grouting engineering, the addition of PNC803 alone can satisfy the requirements for the bleeding rate of the grouting slurry without requiring additional suspension agents to improve the stability of the slurry.

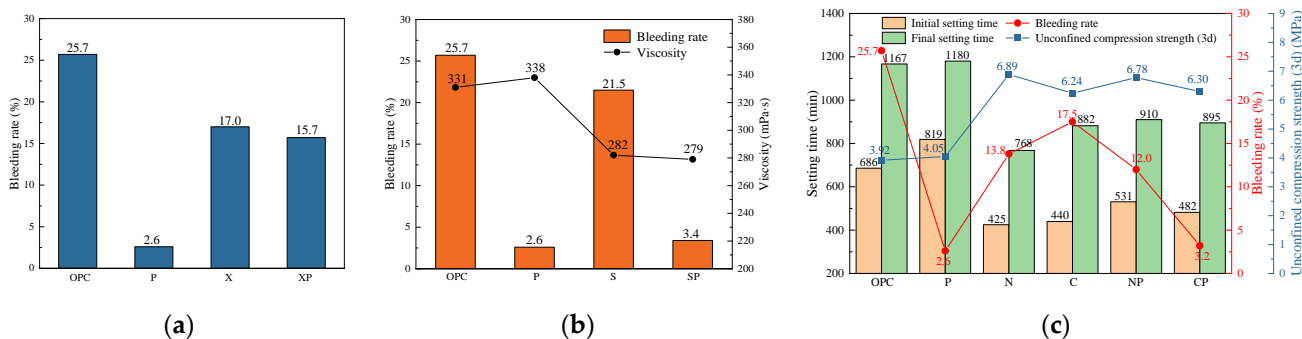


Figure 2. Pre-experimental results: (a) The effects of PNC803 and bentonite on the slurry; (b) the effects of PNC803 and Na_2SO_4 on the slurry; (c) the effect of PNC803 and two types of accelerators on the slurry.

Figure 2b shows that the viscosity and bleeding rate of the SP group cement slurry mixed with PNC803 and Na_2SO_4 were 279 mPa·s and 3.4%, respectively. This was similar to the viscosity of the S group (282 mPa·s) and the bleeding rate of the P group (2.6%). Almost

no negative effect was observed between Na_2SO_4 and PNC803, and when the two acted together, a grouting slurry with a low bleeding rate and viscosity could be obtained. The research by Wang et al. [37] indicated that sulfates do not react with the active substances in CCCW materials, nor do they alter the mechanism of action of CCCW on cement-based materials, which is consistent with the results of this experiment.

Figure 2c shows that when added separately to the cement slurry, the N-type accelerator (NaCl and TEA) was superior to the C-type accelerator (CaCl_2 and TIPA) in terms of the setting time, unconfined compression strength, and bleeding rate. However, when the two types of accelerators were mixed with PNC803, the initial and final setting times of the NP group slurry were extended by 24.9% and 18.5%, respectively, compared with those of the N group slurry, and the unconfined compression strength of the hardened grouting material at 3 d decreased compared with that of the N group. The initial and final setting times of the CP group slurry were only extended by 9.5% and 1.5%, respectively, compared with those of the C group slurry, and the unconfined compression strength at 3 d increased compared with that of the C group. In addition, the bleeding rate of the NP group slurry was relatively high, and its stability was poor, whereas the bleeding rate of the CP group slurry was relatively low and close to that of the P group slurry. The simultaneous presence of the N-type accelerator and PNC803 in the cement slurry reduced their respective effects, whereas almost no negative impact occurred between the C-type accelerator and PNC803, and even a certain synergistic effect was produced in terms of the unconfined compression strength. Therefore, a C-type accelerator was selected for subsequent orthogonal experiments.

3.2. Orthogonal Experiment

Taking the PNC803 dosage as factor A, Na_2SO_4 dosage as factor B, and accelerator ($\text{CaCl}_2:\text{TIPA} = 1:0.025$) dosage as factor C, and based on existing research results and previous experimental summaries, three experimental levels were set for each factor. The orthogonal experimental design and results are listed in Table 2, where G0 is the blank control group for the pure cement slurry. The dosage of each factor in the table is the percentage of its mass relative to the cement mass.

Table 2. Orthogonal experimental design and results.

No.	Factors			Results								
	A (%)	B (%)	C (%)	Viscosity (mPa·s)	Bleeding Rate (%)	Setting Time (min)		Permeability Coefficient ($\times 10^{-6}$ cm/s)		UCS (MPa)		
						Initial	Final	7 d	28 d	3 d	7 d	28 d
G0	—	—	—	331	25.7	686	1167	315	94.20	3.92	5.78	11.49
G1	2.4	0.8	1.0	276	7.3	665	1087	15.23	8.21	5.05	7.13	11.81
G2	2.4	1.6	2.0	185	6.3	529	945	14.74	7.78	6.81	9.48	12.90
G3	2.4	2.4	3.0	245	5.6	387	792	13.82	6.76	7.69	10.54	14.71
G4	3.2	0.8	2.0	282	4.9	553	973	10.32	5.16	6.25	8.68	12.68
G5	3.2	1.6	3.0	164	4.4	402	804	7.06	3.08	7.62	10.63	14.78
G6	3.2	2.4	1.0	230	4.7	645	1068	9.67	4.92	6.48	9.01	12.24
G7	4.0	0.8	3.0	297	2.6	448	839	2.59	0.83	7.39	10.24	14.63
G8	4.0	1.6	1.0	179	3.2	676	1102	3.21	1.47	5.96	8.46	12.54
G9	4.0	2.4	2.0	235	2.9	484	886	1.57	0.41	7.34	10.01	14.52

3.2.1. Viscosity

As shown in Table 2, the viscosities of the grouting materials with different proportions varied significantly. Among them, G5 had the lowest viscosity of 164 mPa·s, and G7 had the highest viscosity of 297 mPa·s. Figure 3a shows the range analysis results of the viscosity of each group of slurries. Na_2SO_4 had the greatest impact on slurry viscosity. When the added amount of Na_2SO_4 was 0.8%, the viscosity of the slurry decreased by approximately 15%.

When the added amount was 1.6%, the viscosity of the slurry decreased to approximately 50% of that of the original slurry. However, when the added amount of Na_2SO_4 exceeded 1.6%, the viscosity of the slurry increased rapidly. This is consistent with the test results in reference [38] demonstrating that the viscosity and fluidity of the slurry first increase and then decrease with increases in the sodium sulfate content. This might be because excessive Na_2SO_4 weakened the electrostatic repulsion between cement particles, thereby affecting the expansion and fluidity of the slurry.

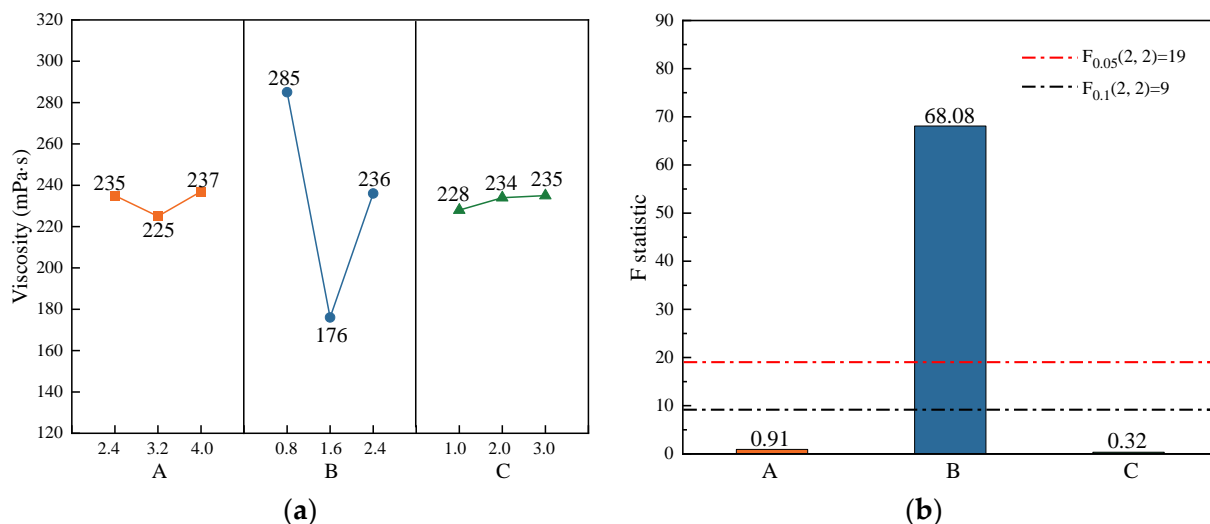


Figure 3. Range and variance analysis of the viscosity: (a) range analysis; (b) variance analysis.

A variance analysis was performed on the orthogonal results to further evaluate the significance of the various factors on the viscosity of the slurry, as shown in Figure 3b. Generally, when the F-statistic value exceeds $F_{0.05}(2, 2)$, the impact of the factor is significant. When the F-statistic value is between $F_{0.05}(2, 2)$ and $F_{0.1}(2, 2)$, the factor has a certain impact. When the F-statistic value is less than $F_{0.1}(2, 2)$, the factor effect is considered insignificant. The results indicated that the degree of influence of the various factors on the viscosity of the slurry was $B > A > C$. Among these factors, the dosage of Na_2SO_4 had a significant impact on the viscosity of the slurry, whereas the dosages of PNC803 and the accelerator had no significant effects on the viscosity. In tunnel anti-seepage grouting engineering, a slurry with a low viscosity is conducive to the diffusion of the slurry in the injected structure. Therefore, for the convenience of the grouting operation, the optimal combination based on viscosity was $A_k B_k C_k$, which meant that the Na_2SO_4 dosage could be utilized at the second level (1.6%), the PNC803 dosage could be utilized at any value within its horizontal k range (2.4–4.0%), and the accelerator dosage could be utilized at any value within its horizontal k range (1.0–3.0%).

3.2.2. Bleeding Rate

Figure 4 shows the influence of each factor on the bleeding rate of the slurry. The F-statistic value of A was much greater than $F_{0.05}(2, 2)$, indicating that the dosage of PNC803 had a significant impact on the bleeding rate of the slurry. This was because the active substances contained in PNC803 promoted the hydration reaction of the originally unhydrated cement in the slurry. On the one hand, it consumed water in the slurry, which to some extent prevented the floating and separation of the cement slurry. On the other hand, the more complete the hydration reaction, the more hydration products were produced, the larger the solid volume, and the lower the bleeding rate. According to Table 2, the slurries of G4–G9 satisfied the requirement for a bleeding rate of less than 5% in grouting engineering [39]. Therefore, from the perspective of slurry stability and cost savings, the optimal combination based on the bleeding rate was $A_2 B_k C_k$.

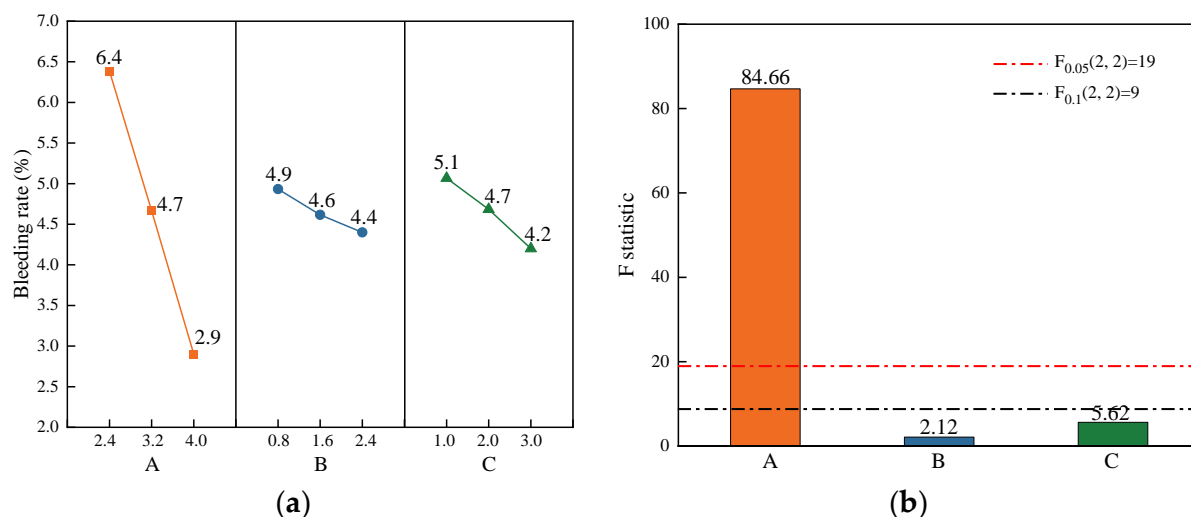


Figure 4. Range and variance analysis of the bleeding rate: (a) range analysis; (b) variance analysis.

3.2.3. Setting Time

As Table 2 shows, the variation range of the slurry setting time was large for different groups. The G3 slurry had the shortest initial and final setting times of 387 and 792 min, respectively. Compared with that of the G0 slurry, these values decreased by 43.6% and 32.1%, respectively. The range and variance analyses of the setting time of the slurry (Figure 5) revealed that PNC803 had almost no effect on the slurry setting time, whereas the combined accelerator of CaCl_2 and TIPA had a significant effect on the slurry setting time. Na_2SO_4 also shortened the setting time; however, its degree of influence was smaller than that of the accelerator. The CaCl_2 in the accelerator underwent a salt effect in the slurry, increasing the solubility of the clinker minerals and accelerating the initial hydration reaction progress of the cement. It can also form complex salts with C_3A , and the presence of complex salts increases the proportion of solid phases in the slurry, thereby promoting slurry hardening. In addition, TIPA has superior surface activity and can enhance cement hydration to generate colloids [40], which is beneficial for improving the compactness of the slurry and shortening the setting time. Therefore, from the perspective of shortening the duration of waterproofing and water treatment, the optimal combination based on the setting time of the slurry was determined to be $\text{A}_k\text{B}_k\text{C}_3$.

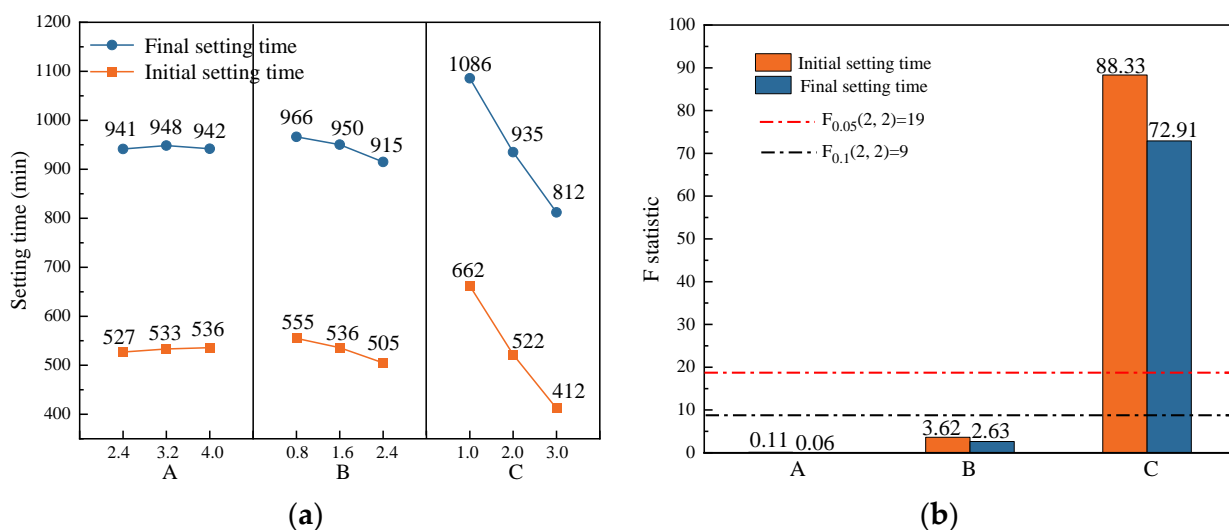


Figure 5. Range and variance analysis of the setting time: (a) range analysis; (b) variance analysis.

3.2.4. Permeability Coefficient

As Table 2 shows, the permeability coefficient of the pure cement slurry grouting body (G0) at 28 d was 9.42×10^{-5} cm/s, whereas the permeability coefficient could be reduced to $10^{-6}\sim 10^{-7}$ cm/s by adding PNC803 and admixtures. Figure 6 shows the range and variance analysis results of the permeability coefficients of the grouted materials at 7 and 28 d. The degree of influence of each additive dosage on the permeability coefficient was A > C > B, among which the influence of the PNC803 dosage on the permeability coefficient was significant. During the solidification of the cement-based slurry, many small cracks and pores were interconnected with each other, forming water channels. Both PNC803 and the admixtures promoted the hydration of cement to varying degrees, increasing the number of crystals in the slurry system, whereas the original water channels were blocked by the growth and expansion of crystals. Therefore, the permeability coefficient of the grouted materials decreased with an increase in the dosage of various factors. In addition, the pores were generally in a moist state or contained liquid water during the early stages of formation. Some of the active substances in PNC803 entered the pore solution through an osmotic pressure gradient, capillary pressure, and concentration difference, catalyzing secondary crystallization reactions, filling pores, and blocking water channels. With an increase in the curing time, the size and moisture content of the pores constantly changed, promoting the continuous entry of active substances into the capillary pores and resulting in continuous catalytic hydration reactions within the pore structure. Therefore, the permeability coefficient of the grouted materials at 28 d was further reduced compared with that at 7 d. Therefore, from the perspective of the anti-seepage reinforcement effect, the optimal combination based on the permeability coefficient of the grouting body was determined to be $A_3B_kC_k$.

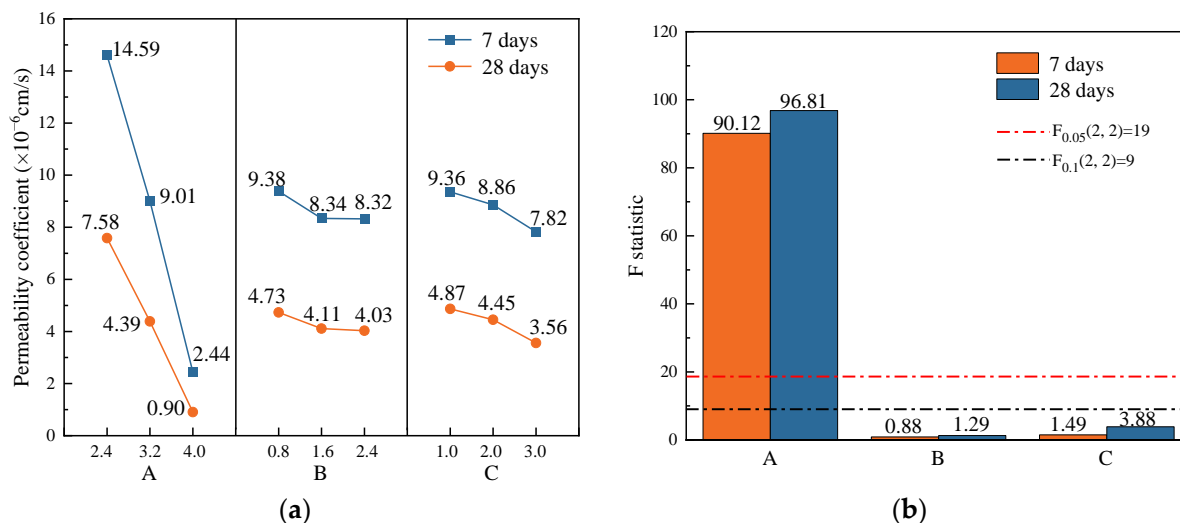


Figure 6. Range and variance analysis of the permeability coefficient: (a) range analysis; (b) variance analysis.

3.2.5. Unconfined Compression Strength

Table 2 shows that, at the optimal quality ratio, the hardened grout's early (3–7 d) strength was approximately twice that of the hardened pure cement grout, whereas its later (28 d) strength was approximately 1.3 times that of the latter. Based on the range analysis and variance analysis of the unconfined compression strength of the slurry stone bodies (Figure 7), all the factors were positively correlated with the unconfined compression strength, with an impact degree of C > B > A. Among them, the dosage of the accelerator had a significant impact on the compression strength of stone bodies at various ages, and the dosage of Na_2SO_4 had a certain degree of influence on the early compression strength of the stone bodies. This was because CaCl_2 and Na_2SO_4 reacted with $\text{Ca}(\text{OH})_2$, reducing the concentration of $\text{Ca}(\text{OH})_2$ in the liquid phase, promoting the early hydration reaction

of cement, and accelerating the precipitation of C-S-H and AFt. C-S-H and AFt played a dominant role in the strength of the structure. TIPA can promote the hydration of C₄AF in solution for a long time [41], thereby promoting later strength growth. Therefore, from the perspective of bearing capacity and durability, the optimal combination based on unconfined compression strength was determined to be A_kB₃C₃.

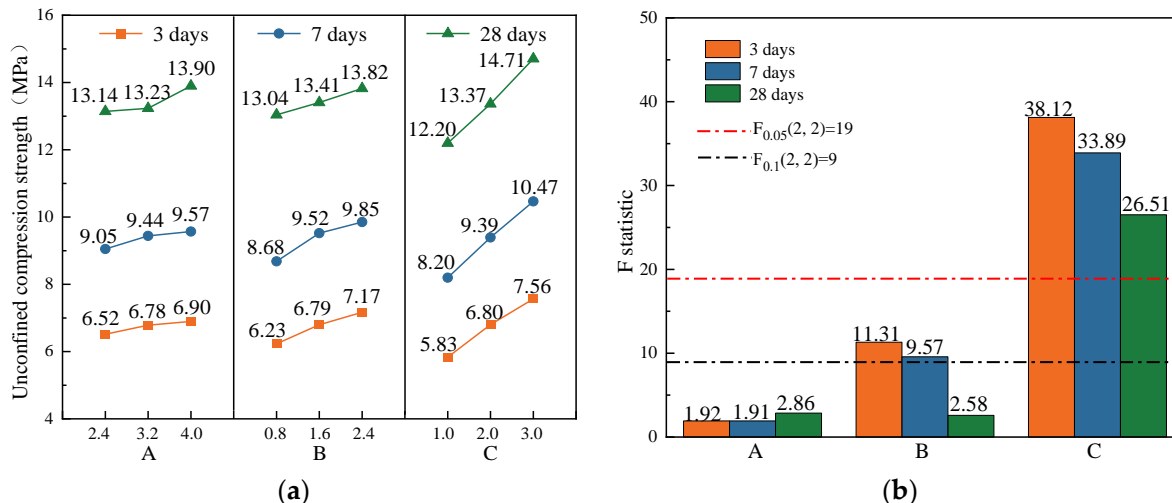


Figure 7. Range and variance analysis of the unconfined compression strength: (a) range analysis; (b) variance analysis.

Based on the various performance factors, the optimal ratio for the high-performance CCCW grouting material was determined to be G5 (A₂B₂C₃), with a PNC803–cement ratio of 3.2%, Na₂SO₄–cement ratio of 1.6%, CaCl₂–cement ratio of 3.0%, and TIPA–cement ratio of 0.075%. Compared with the pure cement slurry, the viscosity of this slurry was reduced by 50%, the bleeding rate was reduced by 83%, the initiate setting time was shortened by approximately 40%, the permeability coefficient (28 d) of the grouting body was reduced to 3.08×10^{-6} cm/s, and the early unconfined compression strength of the hardened grout increased by approximately one time.

3.3. Phase Composition and Microstructure Analysis

3.3.1. XRD

The material compositions of the G0 and G5 hardened grouts were analyzed using XRD, as shown in Figure 8. The main components detected in G0 were Ca(OH)₂, C-S-H, CaCO₃, and C₃A. In addition to detecting the same hydration products, Ca(OH)₂ and C-S-H, as in G0 in G5, some AFt crystals and hydrated calcium borate crystals were observed. Ca(OH)₂ is frequently enriched and crystallized into coarse grains in the interface transition zone, which limits the development of the mechanical properties of cement-based materials [42]. Based on the relative intensity of the diffraction peaks, the diffraction peak intensity of Ca(OH)₂ in G5 decreased relative to that of C-S-H. This suggests that, during the reaction process, the high-performance capillary crystalline slurry system consumed unfavorable Ca(OH)₂ to a certain extent. In addition, in the presence of sulfate ions, the solubility of C₃A increased, increasing the number of AFt crystals in the cement-based slurry system. A certain amount of AFt can fill capillary pores and cracks, which is beneficial for improving the density and strength of the stone body and can also compensate for the shrinkage deformation of the stone body. However, it is worth mentioning that excessive AFt can cause internal expansion and deformation of the structure, ultimately leading to damage. Therefore, it is necessary to control the dosage of sulfate added [37]. Hydrated calcium borate may be produced by PNC803 during its action in the slurry. Owing to its needle-like and radial crystal structure, its existence may play a role similar to that of AFt.

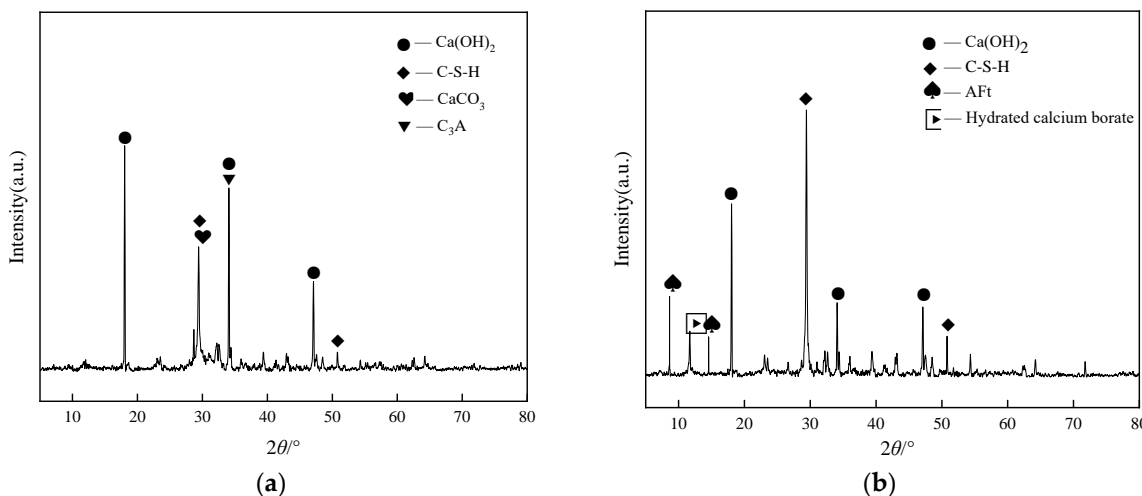


Figure 8. XRD patterns: (a) G0; (b) G5.

3.3.2. CT Results

The G0 and G5 grouted materials with different curing ages were scanned using an industrial CT to obtain the main parameters of the pore structure of each group of samples. The resolution was limited by the testing equipment, so the minimum pore diameter that could be identified is 0.22mm. As shown in Figure 9a, the total porosity of G5 at 3, 7, and 28 d decreased by more than 40% compared with that of G0. Due to the irregular development of the pore morphology, the equivalent diameter [43,44] was used to characterize the pore structure morphology. The principle of equivalence is to transform an irregular pore into a regular sphere. By using the sphere volume formula, the equivalent diameter can be obtained by reverse calculating the pore volume obtained using VG Studio MAX 2.0 software [45]. To gain a clearer understanding of the changes in the pore sizes within the grouted materials, the pores were divided into six equivalent diameter ranges: <4, 4–4.8, 4.8–5.6, 5.6–6.4, 6.4–7.2, and >7.2 mm. The percentage of the pore volume in each range relative to the total pore volume was calculated, and the results are shown in Figure 9b. Compared with G0, the volume proportion of pores with an equivalent diameter of less than 4 mm in G5 significantly increased at different curing ages, by about 22%. The volume proportion of pores with an equivalent diameter of 6.4 mm or more significantly decreased, with a decrease of about 5% in the range of 6.4–7.2 mm and a decrease of about 20% in the range of >7.2 mm. To compare the changes in the pore distribution inside the G0 and G5 structures, a three-dimensional image reconstruction operation was performed on the internal structure of the grouted materials, as shown in Figure 9c. The G0 structure had a large number of pores and a wide distribution range, with larger interconnected pores. In contrast, G5 had fewer pores and a smaller pore volume after curing for 3 and 28 d. The presence of crystalline substances changed the internal spatial structure, reduced the number of pores, and refined the pores in the slurry. The pores were broken from larger pores to smaller pores with an equivalent diameter of less than 4 mm, which to some extent reduced the water passage inside the structure and improved the compactness. This explained the improved impermeability and mechanical properties of the slurry consolidation body.

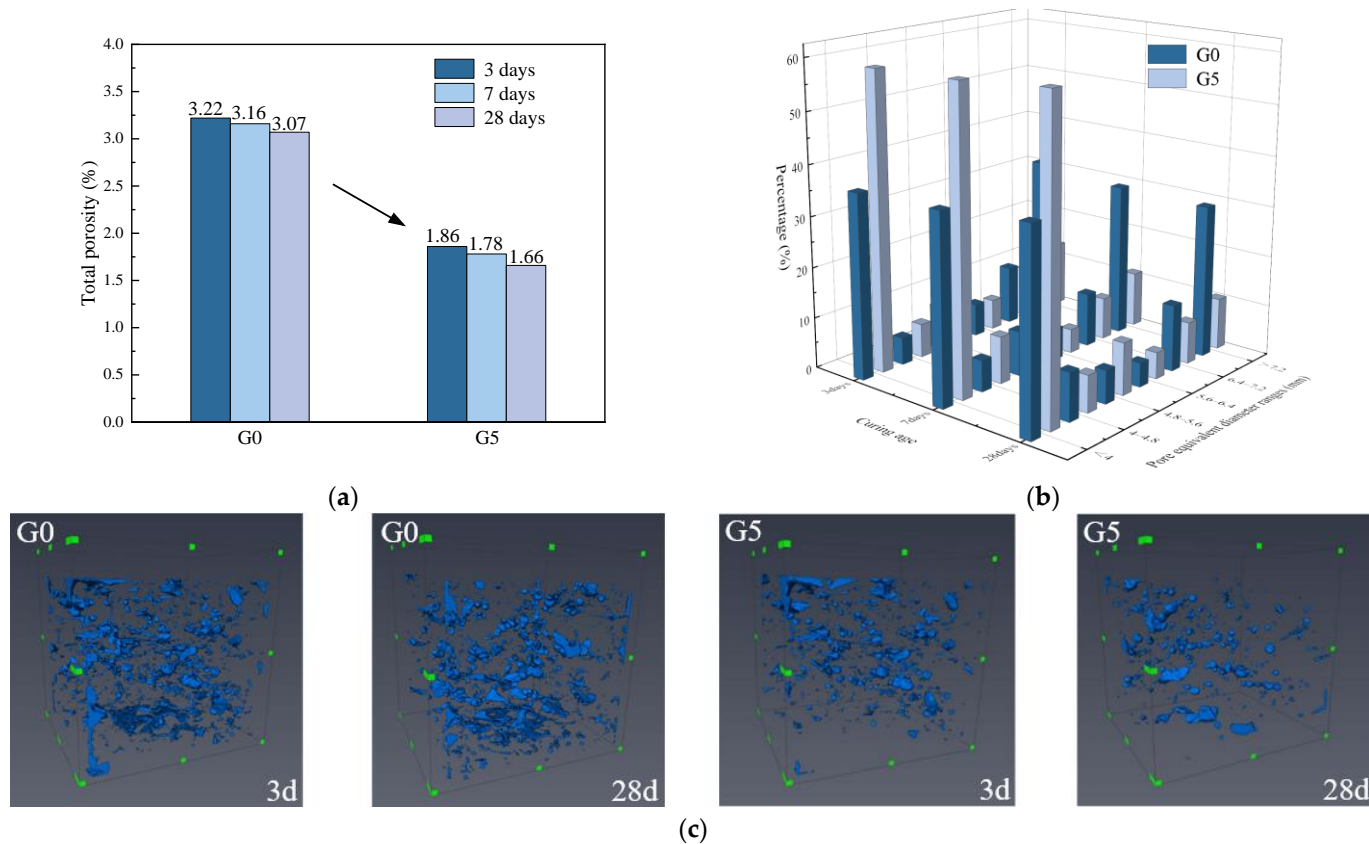


Figure 9. Comparison of internal pores in G0 and G5 grouting bodies: (a) total porosity; (b) pore size distribution; (c) pore characteristics.

3.3.3. SEM Results

SEM was performed on the G0 and G5 hardened grouts at magnifications of 300, 5000, and 10,000 times to further reveal the action mechanism of the high-efficiency CCCW grouting material, as shown in Figure 10. A significant difference was observed in the microstructure between G0 and G5. The interior structure of the G0 sample was comparatively loose, with interconnected fissures and voids. Consistent with the XRD results, flaky $\text{Ca}(\text{OH})_2$, fibrous C-S-H gel, and unhydrated cement particles were observed in the G0 sample. However, in the structure of the G5 stone body, a large number of needle- and vine-like crystals were observed, namely C-S-H gel, AFt crystals, and hydrated calcium borate crystals. These crystalline substances grew radially into the pores and crossed to form a three-dimensional network structure connecting the dispersed cement particles and their hydration products. When the slurry was injected into the structural cracks, the water-soluble active substances in the capillary crystalline material entered the concrete structure with water as the medium, generating more Ca^{2+} complexes. The anions in the complexes could be replaced by SiO_3^{2-} , CO_3^{2-} , and $\text{Al}(\text{OH})_4^-$, producing more stable precipitates [46]. On the one hand, in the process of slurry consolidation, these gels and crystals can be used as substrate materials to reduce the potential energy barrier that must be overcome for slurry solidification, thereby accelerating the setting and solidification of the slurry and improving the early strength of the consolidated body. On the other hand, they can fill the small cracks and capillary pores, improve the overall density of the structure, and hinder the invasion of water and other harmful substances, thereby enhancing the impermeability and corrosion resistance of the structure. In addition, since the catalysts in the capillary crystalline material are not consumed in chemical reactions [27], this slurry can provide permanent impermeability and waterproofing protection for concrete structures.

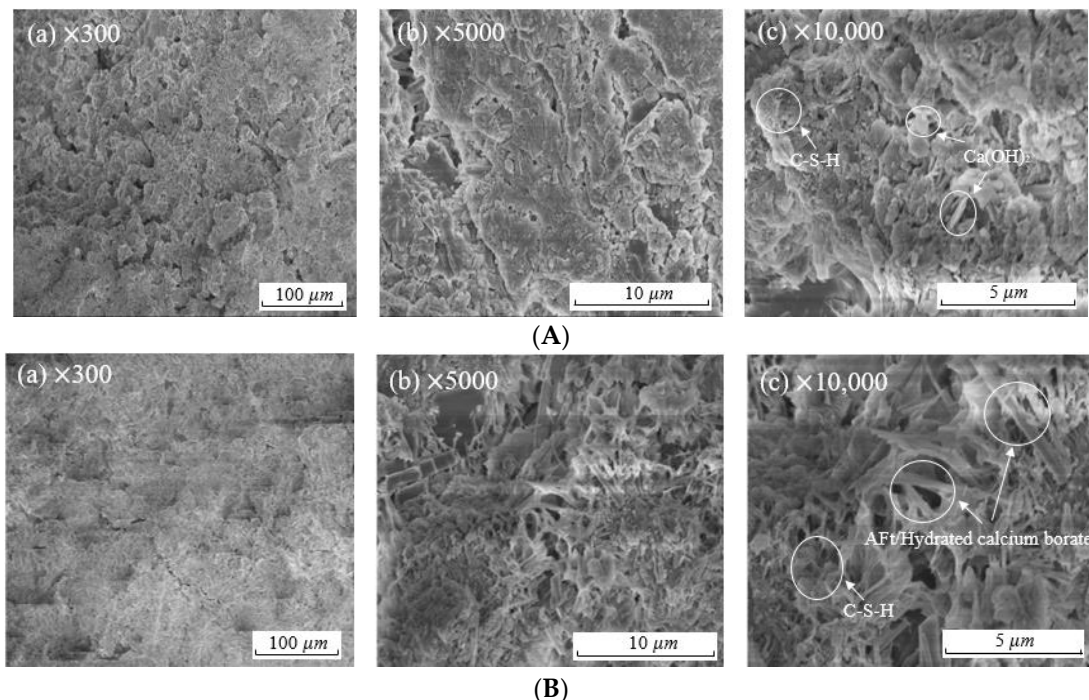


Figure 10. SEM images: (A) G0; (B) G5.

4. Conclusions

In this study, experiments were conducted using cement, capillary crystalline materials, and admixtures as raw materials to obtain a reasonable proportion scheme for high-performance CCCW grouting material. The phase composition, pore structure, and microstructure were analyzed using XRD, CT, and SEM. The following are the main conclusions obtained:

- (1) When the capillary crystalline material PNC803 is added to the cement-based slurry with bentonite, sodium chloride, and TEA, their respective effects on the slurry are weakened. However, PNC803 exhibits good synergistic effects with sulfate, calcium chloride, and TIPA.
- (2) A reasonable quality ratio for this high-efficiency cement-based capillary crystalline grouting material is water/cement/PNC803/sodium sulfate/calcium chloride/TIPA = 1:1:0.032:0.016:0.03:0.00075. Its viscosity is 164 mPa·s, its bleeding rate is 4.4%, and the initial setting time and final setting time are 402 and 804 min, respectively. The permeability coefficients of the grouted materials at 7 and 28 d are 7.06×10^{-6} and 3.08×10^{-6} cm/s, respectively. The compression strengths of the hardened grout at 3, 7, and 28 d are 7.62, 10.63, and 14.78 MPa, respectively.
- (3) The enhancement in the impermeability of the grouted material is related to the improvement in the internal pore structure. The crystalline products in the slurry effectively fill the larger pores within the structure, further refining the pores in the slurry and blocking water passage inside the structure, thereby improving the impermeability.
- (4) The capillary crystalline material PNC803 and cement admixtures promote cement hydration in different ways, producing numerous C-S-H gels, AFt crystals, and hydrated calcium borate crystals. These substances can serve as crystallization centers, reducing the solidification energy barrier of the slurry and accelerating the setting and hardening of the cement. In addition, they can play reinforcing, skeletal, and filling roles in pores, thereby improving the strength and density of cured structures.
- (5) This article only studied the slurry's performance parameters as an anti-seepage grouting material and did not determine the grouting parameters of the slurry during the construction process. Therefore, subsequent research will analyze the effects of

factors such as the grouting pressure, grouting time, and rock friction coefficient on the grouting effect using model experiments and numerical simulations.

Author Contributions: Conceptualization, M.W. and X.Y.; methodology, K.Z.; validation, K.Z.; formal analysis, X.Y.; investigation, K.Z.; resources, K.Z.; data curation, R.C.; writing—original draft preparation, M.W.; writing—review and editing, M.W. and X.Y.; visualization, R.C.; supervision, X.Y.; project administration, X.Y.; funding acquisition, X.Y. All authors have read and agreed to the published version of the manuscript.

Funding: This research was funded by the Fundamental Research Funds for the Central Universities, grant number 300102219219.

Data Availability Statement: The data used to support the findings of this study are available from the corresponding author upon request. The data are not publicly available due to privacy.

Conflicts of Interest: Author Kunlong Zheng was employed by the company China State Construction Silk Road Investment Group Co., Ltd. The remaining authors declare that the research was conducted in the absence of any commercial or financial relationships that could be construed as a potential conflict of interest.

References

1. Gong, X.N.; Guo, P.P. Prevention and mitigation methods for water leakage in tunnels and underground structures. *China J. Highw. Transp.* **2021**, *34*, 1–30. (In Chinese) [[CrossRef](#)]
2. Chang, Z.; Mei, H.P.; Yan, C.G.; Shi, Y.L.; Zhu, X.M.; Lu, Z.F.; Jia, Z.L. Health status evaluation of highway tunnel inverted arch based on variable weight and extension cloud model. *Eng. Fail. Anal.* **2024**, *157*, 107939. [[CrossRef](#)]
3. Chakrabarti, S.; Banerjee, S.; Chaudhuri, B.; Bhattacharjee, S.; Dutta, B.K. Application of biodegradable natural polymers for flocculated sedimentation of clay slurry. *Bioresour. Technol.* **2008**, *99*, 3313–3317. [[CrossRef](#)] [[PubMed](#)]
4. Nosrati, A.; Addaimensah, J.; Skinner, W. Rheological behavior of muscovite clay slurries: Effect of water quality and solution speciation. *Int. J. Miner. Process.* **2012**, *102*, 89–98. [[CrossRef](#)]
5. Zhang, C.; Yang, J.; Ou, X.; Fu, J.; Xie, Y.; Liang, X. Clay dosage and water/cement ratio of clay-cement grout for optimal engineering performance. *Appl. Clay Sci.* **2018**, *163*, 312–318. [[CrossRef](#)]
6. Yang, X.H.; Yu, Y.H. Application of cement-silicate double solution grouting in loess tunnel construction. *China J. Highw. Transp.* **2004**, *2*, 69–73. (In Chinese) [[CrossRef](#)]
7. Ye, F.; Sun, C.H.; Mao, J.H.; Han, X.; Chen, Z. Analysis on grouting mechanism for shield tunnel segment by cement and sodium silicate mixed grout mixed grout in consideration of time-dependency and space effect of viscosity. *China J. Highw. Transp.* **2017**, *30*, 49–56. (In Chinese) [[CrossRef](#)]
8. Li, S.C.; Sha, F.; Liu, R.T.; Zhang, Q.S.; Li, Z.F. Investigation on fundamental properties of microfine cement and cement-slag grouts. *Constr. Build. Mater.* **2017**, *153*, 965–974. [[CrossRef](#)]
9. Mozumder, R.A.; Laskar, A.I.; Hussain, M. Penetrability prediction of microfine cement grout in granular soil using Artificial Intelligence techniques. *Tunn. Undergr. Space Technol.* **2018**, *72*, 131–144. [[CrossRef](#)]
10. Shin, E.C.; Park, J.J.; Yu, J.; Patra, C.R. Prediction of Grouting Efficiency by Injection of Cement Milk into Sandy Soil Using an Artificial Neural Network. *Soil Mech. Found. Eng.* **2018**, *55*, 305–311. [[CrossRef](#)]
11. Sha, F.; Li, S.C.; Liu, R.T.; Zhang, Q.S.; Li, Z.F.; Liu, H.J. Performance and engineering application of effective microfine cement-based grout for water-rich sand strata. *Chin. J. Rock Mech. Eng.* **2019**, *38*, 1420–1433. (In Chinese) [[CrossRef](#)]
12. Li, H.Y.; Zhou, A.X.; Wu, Y.F.; Deng, L.; Zhu, K.C.; Lu, F. Research and Development of Self-Waterproofing Concrete for Tunnel Lining Structure and Its Impermeability and Crack Resistance Characteristics. *Materials* **2023**, *16*, 5557. [[CrossRef](#)]
13. Yan, D.; Lai, L.P.; Xiao, X.D.; Zhang, L.; Zhao, Z.L.; Zhao, J. Water Consolidation Performance of Acrylic-Polymer-Modified Materials and Their Concrete Impermeability Repair Characteristics. *Gels* **2023**, *9*, 764. [[CrossRef](#)] [[PubMed](#)]
14. Wang, W.Z.; Zhao, W.Q.; Zhang, J.J.; Zhou, J.H. Epoxy-based grouting materials with super-low viscosities and improved toughness. *Constr. Build. Mater.* **2020**, *267*, 121104. [[CrossRef](#)]
15. Wang, Y.X.; Liu, Q.S. Investigation on fundamental properties and chemical characterization of water-soluble epoxy resin modified cement grout. *Constr. Build. Mater.* **2021**, *299*, 123877. [[CrossRef](#)]
16. Liu, W.T.; Sun, Y.D.; Meng, X.X.; Qin, Y.Y. Experimental analysis of Nano-SiO₂ modified waterborne epoxy resin on the properties and microstructure of cement-based grouting materials. *Energy* **2023**, *268*, 126669. [[CrossRef](#)]
17. Naudts, A. Irreversible changes in the grouting industry caused by polyurethane grouting: An overview of 30 years of polyurethane grouting. In Proceedings of the 3rd International Conference on Grouting and Ground Treatment, Reston, VA, USA, 10–12 February 2003; pp. 1266–1280.
18. Saleh, S.; Yunus, N.Z.M.; Ahmad, K.; Ali, N. Improving the strength of weak soil using polyurethane grouts: A review. *Constr. Build. Mater.* **2019**, *202*, 738–752. [[CrossRef](#)]

19. Hao, M.M.; Li, X.L.; Zhong, Y.H.; Zhang, B.; Wang, F.M. Experimental Study of Polyurethane Grout Diffusion in a Water-Bearing Fracture. *J. Mater. Civil. Eng.* **2021**, *33*, 04020485. [[CrossRef](#)]
20. Sun, Y.; Zhao, Y.; Zhang, D.L. Research on application of waterborne capillary crystalline waterproof material in tunnel engineering. *J. China Railw. Soc.* **2018**, *40*, 137–145. (In Chinese) [[CrossRef](#)]
21. Zheng, K.L.; Yang, X.H.; Chen, R.; Xu, L.X. Application of a capillary crystalline material to enhance cement grout for sealing tunnel leakage. *Constr. Build. Mater.* **2019**, *214*, 497–505. [[CrossRef](#)]
22. Li, Z.C.; Huang, F.; Yang, Y.Y.; Xiong, Y.F.; Su, F.; Wang, Y.J.; Tian, X. Improving the Anti-washout Property of Acrylate Grouting Material by Bentonite: Its Characterization, Improving Mechanism, and Practical Application. *Polymers* **2023**, *15*, 3865. [[CrossRef](#)] [[PubMed](#)]
23. Ebigbo, A.; Phillips, A.; Gerlach, R.; Helmig, R.; Cunningham, A.B.; Class, H.; Spangler, L.H. Darcy-scale modeling of microbially induced carbonate mineral precipitation in sand columns. *Water Resour. Res.* **2012**, *48*, W07519. [[CrossRef](#)]
24. Van Wijngaarden, W.K.; Van Paassen, L.A.; Vermolen, F.J.; Van Meurs, G.A.M.; Vuik, C.A. Reactive Transport Model for Biogrout Compared to Experimental Data. *Transp. Porous Media* **2016**, *111*, 627–648. [[CrossRef](#)]
25. Dong, B.Q.; Fang, G.H.; Wang, Y.S.; Liu, Y.Q.; Hong, S.X.; Zhang, J.C.; Lin, S.M.; Xing, F. Performance recovery concerning the permeability of concrete by means of a microcapsule based self-healing system. *Cem. Concr. Compos.* **2017**, *78*, 84–96. [[CrossRef](#)]
26. Zheng, G.; Huang, J.Y.; Diao, Y.; Ma, A.Y.; Su, Y.M.; Chen, H. Formulation and performance of slow-setting cement-based grouting paste (SCGP) for capsule grouting technology using orthogonal test. *Constr. Build. Mater.* **2021**, *302*, 124204. [[CrossRef](#)]
27. Zhang, L.Q.; Yu, J.L.; Wang, Y.Y.; Han, B.G.; Chen, M.C.; Xu, K.C. Study on cementitious composites with permeable crystalline agent: A review. *Mater. Rep.* **2024**, *38*, 22100014. (In Chinese)
28. Yang, X.H.; Zheng, K.L.; Xu, L.X. Experiment on effect of capillary crystalline material additives on cement slurry performance. *China J. Highw. Transp.* **2019**, *32*, 129–135. (In Chinese) [[CrossRef](#)]
29. Liu, P.; Liu, M.L.; Sha, F.; Chen, Y.; Zhi, W.T.; He, S.S.; Yu, Z.W. Preparation and performance investigation of a high efficiency cement permeation type waterproofing materials. *Constr. Build. Mater.* **2022**, *365*, 130140. [[CrossRef](#)]
30. Qi, M.; Pu, Y.D.; Yang, S.; Sheng, K.; Yuan, X.Y. Effect of graphene oxide on the impermeability of cementitious capillary crystalline waterproofing. *Acta Mater. Compos. Sin.* **2023**, *40*, 1598–1610. (In Chinese) [[CrossRef](#)]
31. Li, X.W. Research on the Composition and Properties of Cementitious Capillary Crystalline Waterproofing Coating Mixture. Master’s Thesis, Chongqing University, Chongqing, China, 2006. (In Chinese). [[CrossRef](#)]
32. Tang, C.J. Research on Cementitious Capillary Crystalline Waterproofing Coating Mixture. Master’s Thesis, South China University of Technology, Guangzhou, China, 2009. (In Chinese). [[CrossRef](#)]
33. JJG 1002-2005; Verification Regulation of Rotational Viscometers. General Administration of Quality Supervision, Inspection and Quarantine of the People’s Republic of China. Standards Press of China: Beijing, China, 2005.
34. JTJ 3420-2020; Testing Methods of Cement and Concrete for Highway Engineering. Ministry of Transport of the People’s Republic of China; Standards Press of China: Beijing, China, 2020.
35. GB/T 1346-2011; Test Methods for Water Requirement of Normal Consistency, Setting Time and Soundness of the Portland Cement. General Administration of Quality Supervision, Inspection and Quarantine of the People’s Republic of China. Standards Press of China: Beijing, China, 2011.
36. GB/T 50081-2019; Standard for Test Methods of Concrete Physical and Mechanical Properties. Ministry of Housing and Urban-Rural Development of the People’s Republic of China; State Administration for Market Regulation. China Architecture and Building Press: Beijing, China, 2019.
37. Wang, C.H.; Xiao, J.; Zhang, Q.H.; Shi, J.Y.; Zhang, Z.D.; Long, C.Y. Influences of the joint action of sulfate erosion and cementitious capillary crystalline waterproofing materials on the hydration products and properties of cement-based materials: A review. *J. Build. Eng.* **2023**, *68*, 106061. [[CrossRef](#)]
38. Cui, D.X.; Qin, H.G.; Guo, W.; Pan, W.Y.; Yang, Y.W. The influence of Na₂SO₄ content in water reducing agents on the performance of concrete. *Chin. Concr. Cem. Prod.* **2009**, *4*, 18–20. (In Chinese) [[CrossRef](#)]
39. Yang, X.D. *Technical Manual of Anchorage and Grouting*; China Electric Power Press: Beijing, China, 2009; pp. 319–320.
40. Huang, H.; Li, X.R.; Shen, X.D. Hydration of ternary cement in the presence of triisopropanolamine. *Constr. Build. Mater.* **2016**, *111*, 513–521. [[CrossRef](#)]
41. Gartner, E.; Myers, D. Influence of Tertiary Alkanolamines on Portland Cement Hydration. *J. Am. Ceram. Soc.* **1993**, *76*, 1521–1530. [[CrossRef](#)]
42. Li, G.Y.; Huang, X.F.; Lin, J.S.; Jiang, X.; Zhang, X.Y. Activated chemicals of cementitious capillary crystalline waterproofing materials and their self-healing behavior. *Constr. Build. Mater.* **2019**, *200*, 36–45. [[CrossRef](#)]
43. Wang, G.; Shen, J.N.; Chu, X.Y.; Cao, C.J.; Jiang, C.H.; Zhou, X.H. Characterization and analysis of pores and fissures of high-rank coal based on CT three-dimensional reconstruction. *J. China Coal Soc.* **2017**, *42*, 2074–2080. (In Chinese) [[CrossRef](#)]
44. Huang, D.; Gao, Y.K.; Huang, W.B. Research on pore structural change of gravel soil under seepage erosion based on CT scanning. *Hydrogeol. Eng. Geol.* **2024**, *51*, 123–131. (In Chinese) [[CrossRef](#)]

45. Liu, Z.X.; Dong, S.N.; Nan, S.H.; Zhang, D.Y.; Liu, D. Micro-CT analysis of void characteristics at the top of middle ordovician limestone in Hanxing mining area. *J. Min. Saf. Eng.* **2021**, *38*, 343–352. (In Chinese) [[CrossRef](#)]
46. Kuang, Y.C.; Ou, J.P. Experiment and research on permeable crystallization self-repairing performance of concrete. *J. Railw. Sci. Eng.* **2008**, *1*, 6–10. (In Chinese) [[CrossRef](#)]

Disclaimer/Publisher’s Note: The statements, opinions and data contained in all publications are solely those of the individual author(s) and contributor(s) and not of MDPI and/or the editor(s). MDPI and/or the editor(s) disclaim responsibility for any injury to people or property resulting from any ideas, methods, instructions or products referred to in the content.